of 5 μK in the $F = 3$ state, using a two-dimensional magneto-optical trap (2D-MOT) to load a 3D-MOT through a differential pumping stage. We ran the interferometer with a pulse separation time of T = 15.5 ms and identified the two outputs separately via fluorescence detection with a camera (*14*).

Figure 2A shows an interference fringe obtained by measuring the atom number at the two interferometer outputs while varying the phase $\Delta\phi$ (*13*, *14*). Fitting the fringe with a sine wave determines the total acceleration of the atoms. To take out systematic effects, we applied wavevector reversal (i.e., we changed the direction of the photon impulse). This inverts the signal produced by accelerations, but many systematic effects remain unchanged and can be taken out (*29*). To measure the acceleration a originating from atom-sphere interactions (our signal for chameleons) separately from Earth's gravitational acceleration g, we compared the total acceleration $a_{tot} = a + g$ with the sphere located in the "near" position with g measured with the sphere in the "far" position. "Near" means an effective vertical distance of 8.8 mm from the surface of the sphere, and "far" means about 3 cm to the side.

One measurement consists of four interference fringes: two with the wavevector normal (one each with the sphere near and far) and two with the wavevector inverted (as above). Fifty such measurements with their statistical error bars are shown in Fig. 2B. For each, we averaged the acceleration as measured with normal and inverted wavevectors to eliminate systematic effects, and we compared the acceleration thus measured between the near and far positions of the sphere. Figure 2C shows a histogram of these acceleration differences. Fitting a Gaussian distribution to the histogram resulted in an estimate of $a = 2.7 \pm 3.3\ \mu m/s^2$. We added corrections for systematic ac Stark shifts, magnetic fields, and electrostatic fields (*13*) (table S1) and arrived at $a = -0.7 \pm 3.7\ \mu m/s^2$. The negative sign indicates acceleration away from the sphere. The 2σ (95%) confidence interval for these data is $-8.2\ \mu m/s^2 < a < 6.8\ \mu m/s^2$.

A chameleon has a spin of 0 and can therefore only produce attractive forces (assuming universal coupling to matter). A one-tailed test shows $a < 5.5\ \mu m/s^2$ at the 95% confidence level. Comparison to the expected acceleration (Eqs. S8 to S11) yields the excluded range of parameters Λ and M, shown in Fig. 3A. Our experiments excluded chameleons at the scale of the cosmological constant $\Lambda = \Lambda_0 = 2.4$ meV for $M < 2.3 \times 10^{-5}\ M_{Pl}$, making the most conservative assumption of $\xi = 0.55$ for a parameter ξ entering Eqs. S9 and S10 that describes the influence of the vacuum chamber walls (*14*). This result rules out chameleons that would reproduce the observed acceleration of the cosmos. To place our result in the context of previous experiments, we assumed that $\Lambda = \Lambda_0$. Figure 3B shows the excluded region for different values of the exponent n, and Fig. 3C shows the excluded region compared with experiments that assume photon-chameleon coupling (our results do not rely on such a coupling). In short, the only chameleon theories that are still viable are the white areas in Fig. 3, A to C, all of which we have narrowed by several orders of magnitude by using atom interferometry.

Our analysis can be generalized to constrain other scalar field theories, such as symmetron, varying-dilaton, and $f(R)$ theories. These theories belong to the same universality class as the chameleon theories, in that their screening effect is triggered by the local scalar field value, as opposed to its spatial derivatives. As a result, their phenomenology is similar to that of the chameleon (*7*).

REFERENCES AND NOTES

1. Planck Collaboration, http://xxx.lanl.gov/abs/1502.01589 (2015).
2. C. Wetterich, *Nucl. Phys. B* **302**, 668–696 (1988).
3. P. J. E. Peebles, B. Ratra, *Astrophys. J.* **325**, L17 (1988).
4. J. A. Frieman, C. T. Hill, A. Stebbins, I. Waga, *Phys. Rev. Lett.* **75**, 2077–2080 (1995).
5. L. J. Hall, Y. Nomura, S. J. Oliver, *Phys. Rev. Lett.* **95**, 141302 (2005).
6. D. J. Kapner *et al.*, *Phys. Rev. Lett.* **98**, 021101 (2007).
7. A. Joyce, B. Jain, J. Khoury, M. Trodden, *Phys. Rep.* **568**, 1–98 (2015).
8. J. Khoury, A. Weltman, *Phys. Rev. Lett.* **93**, 171104 (2004).
9. D. F. Mota, D. J. Shaw, *Phys. Rev. Lett.* **97**, 151102 (2006).
10. C. Burrage, E. J. Copeland, E. A. Hinds, *J. Cosmol. Astropart. Phys.* **2015**, 042 (2015).
11. M. Kasevich, S. Chu, *Phys. Rev. Lett.* **67**, 181–184 (1991).
12. A. D. Cronin, J. Schmiedmayer, D. E. Pritchard, *Rev. Mod. Phys.* **81**, 1051–1129 (2009).
13. P. Hamilton *et al.*, *Phys. Rev. Lett.* **114**, 100405 (2015).
14. See the supplementary materials on *Science* Online.
15. P. Brax, C. van de Bruck, A. C. Davis, J. Khoury, A. Weltman, *Phys. Rev. D Part. Fields Gravit. Cosmol.* **70**, 123518 (2004).
16. I. Zlatev, L. M. Wang, P. J. Steinhardt, *Phys. Rev. Lett.* **82**, 896–899 (1999).
17. P. Brax, C. Burrage, *Phys. Rev. D Part. Fields Gravit. Cosmol.* **83**, 035020 (2011).
18. D. M. Harber, J. M. Obrecht, J. M. McGuirk, E. A. Cornell, *Phys. Rev. A* **72**, 033610 (2005).
19. T. Jenke *et al.*, *Phys. Rev. Lett.* **112**, 151105 (2014).
20. H. Lemmel *et al.*, *Phys. Lett.* **743**, 310–314 (2015).
21. A. Upadhye, *Phys. Rev. D Part. Fields Gravit. Cosmol.* **86**, 102003 (2012).
22. J. H. Steffen *et al.*, *Phys. Rev. Lett.* **105**, 261803 (2010).
23. G. Rybka *et al.*, *Phys. Rev. Lett.* **105**, 051801 (2010).
24. V. Anastassopoulosa *et al.*, *Phys. Lett. B* 10.1016/j.physletb.2015.07.049 (2015); www.sciencedirect.com/science/article/pii/S0370269315005596.
25. G. Rosi, F. Sorrentino, L. Cacciapuoti, M. Prevedelli, G. M. Tino, *Nature* **510**, 518–521 (2014).
26. A. Sugarbaker, S. M. Dickerson, J. M. Hogan, D. M. S. Johnson, M. A. Kasevich, *Phys. Rev. Lett.* **111**, 113002 (2013).
27. G. M. Tino, M. A. Kasevich, Eds., *Atom Interferometry* (Proceedings of the International School of Physics "Enrico Fermi," vol. 188, IOS Press, Amsterdam, 2014).
28. M. A. Hohensee, B. Estey, P. Hamilton, A. Zeilinger, H. Müller, *Phys. Rev. Lett.* **108**, 230404 (2012).
29. J. M. McGuirk, G. T. Foster, J. B. Fixler, M. J. Snadden, M. A. Kasevich, *Phys. Rev. A* **65**, 033608 (2002).

ACKNOWLEDGMENTS

We acknowledge important discussions with D. Budker, C. Burrage, A. Charman, Y. Nomura, S. Perlmutter, S. Rajendran, and P. Steinhardt. This work was supported by the David and Lucile Packard Foundation; a Defense Advanced Research Projects Agency Young Faculty Award (no. N66001-12-1-4232); NSF grant PHY-1404566; and NASA grants NNH13ZTT002N, NNH13ZTT002N, and NNH11ZTT001N. P.Has. thanks the Austrian Science Fund (grant J3680). The work of J.K. is supported by the NSF Faculty Early Career Development Program (award PHY-1145525) and the NASA Astrophysics Theory Program (grant NNX11AI95G).

SUPPLEMENTARY MATERIALS

www.sciencemag.org/content/349/6250/849/suppl/DC1
Supplementary Text
Figs. S1 to S4
Tables S1 to S4
Equations S1 to S11
Reference (*30*)

12 February 2015; accepted 25 June 2015
10.1126/science.aaa8883

ASTROPHYSICS

Exclusion of leptophilic dark matter models using XENON100 electronic recoil data

The XENON Collaboration*†

Laboratory experiments searching for galactic dark matter particles scattering off nuclei have so far not been able to establish a discovery. We use data from the XENON100 experiment to search for dark matter interacting with electrons. With no evidence for a signal above the low background of our experiment, we exclude a variety of representative dark matter models that would induce electronic recoils. For axial-vector couplings to electrons, we exclude cross sections above 6×10^{-35} cm^2 for particle masses of $m_\chi = 2$ GeV/c^2. Independent of the dark matter halo, we exclude leptophilic models as an explanation for the long-standing DAMA/LIBRA signal, such as couplings to electrons through axial-vector interactions at a 4.4σ confidence level, mirror dark matter at 3.6σ, and luminous dark matter at 4.6σ.

Dark matter in the form of weakly interacting massive particles (WIMPs) is typically expected to induce nuclear recoils in a terrestrial detector target (*1*) with an annually modulated rate due to the motion of the Earth around the Sun (*2*, *3*). Although such a modulation has been observed by the DAMA/LIBRA collaboration using sodium iodine (*4*), it is difficult to interpret it as a dark matter signal, given the null results from other experiments (*5*).

*The XENON Collaboration authors and affiliations are listed in the supplementary materials.
†Corresponding authors: M. Cervantes and R. F. Lang; e-mail: mcervant@purdue.edu, rafael@purdue.edu

Indeed, dark matter–induced nuclear recoils are excluded by these results unless one invokes models that are fine-tuned to create a signal only in DAMA/LIBRA but not in other experiments (*6*–*8*). In contrast, dark matter–induced electronic recoils appear as a viable explanation for the observed modulation because exclusions of other experiments do not apply directly in this case (*9*, *10*). We use data from the XENON100 detector to rule out this possibility for three different, representative dark matter models.

We interpret data from the XENON100 detector that were acquired between 28 February 2011 and 31 March 2012 for a total exposure of 224.6 live days and 34-kg fiducial mass. We have previously searched this data set for spin-independent (*11*) and spin-dependent (*12*) WIMP-induced nuclear recoils, as well as for axion-induced electronic recoils (*13*). XENON100, located in the Gran Sasso underground laboratory, consists of a liquid xenon target that is operated as a low-background time projection chamber (*14*). Each particle interaction results in two signals: The prompt scintillation signal (S1) is used here for energy estimation, and the delayed ionization signal (S2) allows for three-dimensional vertex reconstruction. Data reduction is performed in order to select single-scatter low-energy (<10 keV) recoils in the fiducial volume, while retaining maximal detector efficiency (*13*, *15*). At low energies, the remaining background of XENON100 is dominated by forward-scattered Compton events, resulting in a flat spectrum with a rate of 5.3 events/(keV·tonne·day) in the fiducial volume (*16*) (data file A1). This rate is more than two orders of magnitude lower than the average background rate of about 1019 events/(keV·tonne·day) reported by DAMA/LIBRA in the same energy interval (*17*, *18*), and even smaller than their reported annual modulation amplitude of (11.2 ± 1.2) events/(keV·tonne·day) (*4*). Because the DAMA/LIBRA collaboration has not published the composition of their background at low energies, we test the minimum dark matter signal that would be required to cause the observed modulation. In this scenario, the constant spectrum is fully attributed to background, and only the modulated part itself is attributed to a 100% modulated dark matter signal (Fig. 1). We ignore the practical difficulties of realizing such a highly modulated signal (*3*, *19*) but conservatively consider it as the case that is most challenging to exclude. The dark matter–induced rate would then be zero on 2 December and twice the measured modulation amplitude on 2 June. It follows that there is an optimized time interval to consider for best sensitivity. To find this interval, the signal expected in XENON100 was simulated for different time intervals centered around 2 June. We take into account uncertainties from counting statistics in XENON100 and DAMA/LIBRA, as well as the systematic uncertainty from the conversion of kilo–electron volt (keV) energy into S1 (*13*). The optimum time interval is found to be 70 live days around 2 June, roughly corresponding to April 2011 to August 2011 (Fig. 1). Our expected sensitivity varies by less than 0.1σ with changes of this interval of ±40 live days.

A relativistic treatment of dark matter–electron scattering shows that keV-scale electronic recoils can only be induced by dark matter particles with masses $m_\chi \gtrsim 1\ \mathrm{GeV}/c^2$ scattering inelastically off electrons with momenta on the order of MeV/c (*9*, *20*). As shown in (*9*), even if the dark matter has tree-level (first-order) interactions only with leptons, loop-induced dark matter–hadron interactions dominate the experimental signatures and make the usual exclusions based on nuclear recoil analyses applicable. Thus, we consider here axial-vector $\vec{A}\otimes\vec{A}$ couplings between dark matter and leptons, since in this case, loop contributions vanish, whereas the WIMP–electron coupling is not suppressed by additional small factors of velocity v or mass ratio m_e/m_χ.

We use Eq. 30 in (*9*), with an additional factor of 2 to account for electron occupancy from spin, to calculate the differential rate for WIMP-electron scattering (data file A2). The expected rate includes a sum over the atomic shells of the target, and for each shell, integrates the momentum wave function of the electrons to get the contribution at a given recoil energy. Given the requirement that the energy deposited in the detector must be more than the binding energy of the electron, the largest contribution to the rate in a sodium iodide target comes from the 3s shell of iodine. The contributions from sodium are two orders of magnitude smaller. The momentum-space wave functions for xenon atoms and iodine anions are nearly identical as a result of their similar electron structure. This has the important consequence that a comparison between sodium iodide and xenon is independent of the dark matter halo. The ratio of the calculated differential rates in xenon and sodium iodide are shown in Fig. 2 as a function of deposited energy, considering the full shell structure. This ratio has negligible dependence on the WIMP mass.

We contrast the DAMA/LIBRA signal, interpreted as WIMPs coupling to electrons through axial-vector interactions, with XENON100 data. The energy spectrum of the modulation amplitude

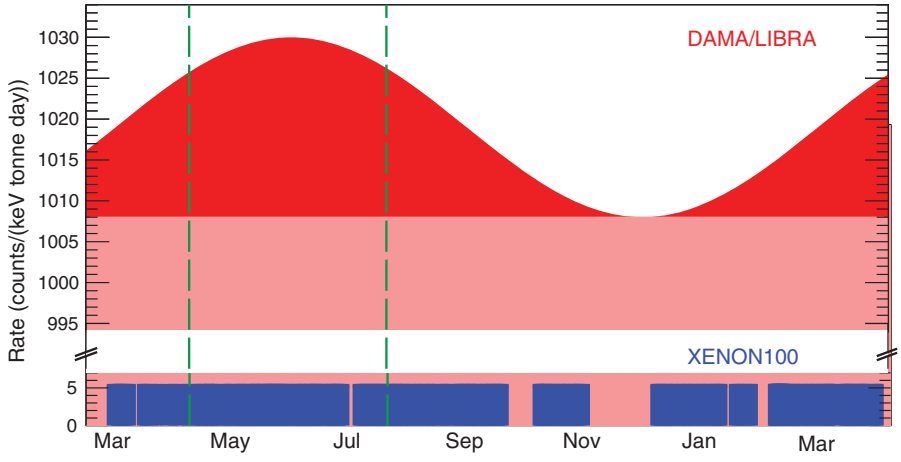

Fig. 1. Conceptual illustration of the analysis. Shown is the DAMA/LIBRA rate (red) (*17*) with the modulated rate in (2 to 6) keV from the fit parameters in (*4*) (dark red). The distribution of the XENON100 live time (blue) is indicated with its average background rate of 5.3 events/(keV·tonne·day), which shows dents due to maintenance or calibration campaigns. The region between the dashed lines (green) indicates the 70 summer live days in which the modulated signal is expected to be largest.

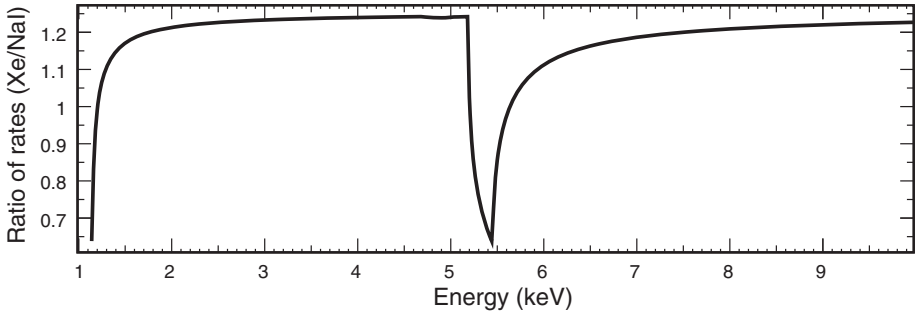

Fig. 2. Calculated ratio of the differential rates in xenon and sodium iodide for inelastic WIMP-electron scattering through axial-vector coupling. The structures around 1 and 5 keV are owing to the small difference in the binding energies of the 3s and 2s shells in xenon and iodine.

(*4*) is multiplied by the energy-dependent ratio from Fig. 2 and by a constant factor of 1.88, which accounts for the time integral of the modulated signal that is expected in our 70 summer live days (Fig. 1). The deposited electronic recoil energy in XENON100 is estimated from the S1 signal, measured in photoelectrons (PE), using the NESTv0.98 model (*21*), which consistently fits the available data (*22*–*25*). The energy scale, shown in (*13*), includes a systematic uncertainty that decreases from 20 to 7% from 1 to 10 keV, reflecting the spread and uncertainties in the measurements. The S1 generation is modeled as a Poisson process and the photomultiplier tube resolution is taken into account in order to obtain the predicted XENON100 S1 spectrum from the scaled energy spectrum (*15*). Our resolution is a factor of 2 worse than that of DAMA/LIBRA; the feature at 5.2 keV in Fig. 2 is lost in this process.

The converted DAMA/LIBRA and measured XENON100 energy spectra are shown in Fig. 3. Part of the DAMA/LIBRA signal is expected to be seen below 2 keV owing to the finite energy resolution of XENON100. The uncertainty in the converted signal includes both the statistical uncertainty in the original DAMA/LIBRA energy spectrum (*4*) and the uncertainties from our energy conversion. The electronic recoil cut acceptance, shown in (*13*), was applied to the converted DAMA/LIBRA spectrum. The uncertainty shown in the XENON100 data is statistical.

The energy region to determine the level of exclusion was chosen starting at the threshold of 3 PE (*11*) to the point where the DAMA/LIBRA signal falls below the expected average XENON100 rate (cyan in Fig. 3, calculated using a flat spectrum background model and scaled for the live time of the data set), which is at 14 PE, corresponding to (2.0 to 5.9) keV. Taking systematic uncertainties into account, a simple comparison of the integral counts in this energy interval excludes the DAMA/LIBRA signal as axial-vector coupling between WIMPs and electrons at 4.4σ significance level, even considering all events from the well-understood XENON100 background (*16*) as signal candidates. To be consistent with previous analyses (*13*), the same data selection cuts were applied. The exclusion remains unchanged if we only impose a minimum set of requirements; namely, that events have a single scatter in the fiducial volume with a prompt S1 and delayed S2 signal in the correct energy range. Furthermore, the exclusion stays above 3σ confidence level even if we consider a 4.5σ downward deviation in the measured data points (*22*–*24*) that are used to set the energy scale, or if we set the light yield in xenon to zero below 2.9 keV, in contradiction with direct measurement (*23*, *24*).

A profile likelihood analysis (*26*) was performed to constrain the cross section $\sigma^0_{\chi e} \equiv G^2 m_e^2/\pi$ for WIMPs coupling to electrons through axial-vector interactions. To this end, we drop the assumption of a 100% modulated rate and use the entire 224.6 live days data set. Fully analogous to (*13*), we use the same energy range and background likelihood function, derived from calibration data. We do not consider energy depositions below 1 keV, the lowest directly measured data point in (*23*). The resulting XENON100 exclusion limit (90% confidence level) is shown (Fig. 4) along with the 1σ/2σ-sensitivity bands based on the background-only hypothesis. It excludes cross sections above 6×10^{-35} cm^2 for WIMPs with a mass of m_χ = 2 GeV/c^2. This is more than five orders of magnitude stronger than the one derived in (*9*) based on data from the XENON10 detector, completely excludes the DAMA/LIBRA signal, and sets the strongest direct limit to date on the cross section

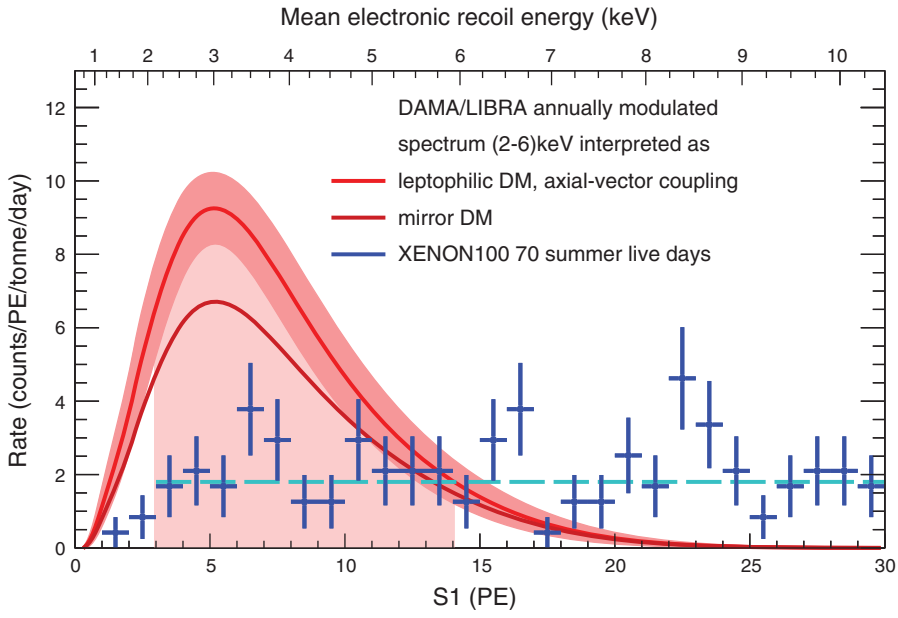

Fig. 3. Contrasting XENON100 data with DAMA/LIBRA. The DAMA/LIBRA modulated spectrum (red), interpreted as WIMPs scattering through axial-vector interactions, as it would be seen in the XENON100 detector. The 1σ band includes statistical and systematic uncertainties. The DAMA/LIBRA modulated spectrum interpreted as luminous dark matter is very similar, whereas the interpretation as mirror dark matter is indicated separately (dark red). The (blue) data points are XENON100 data from the 70 summer live days with their statistical uncertainty. The expected average XENON100 rate is also shown (dashed cyan). The shaded region from (3 to 14) PE was used to quantify the confidence level of exclusion. DM, dark matter.

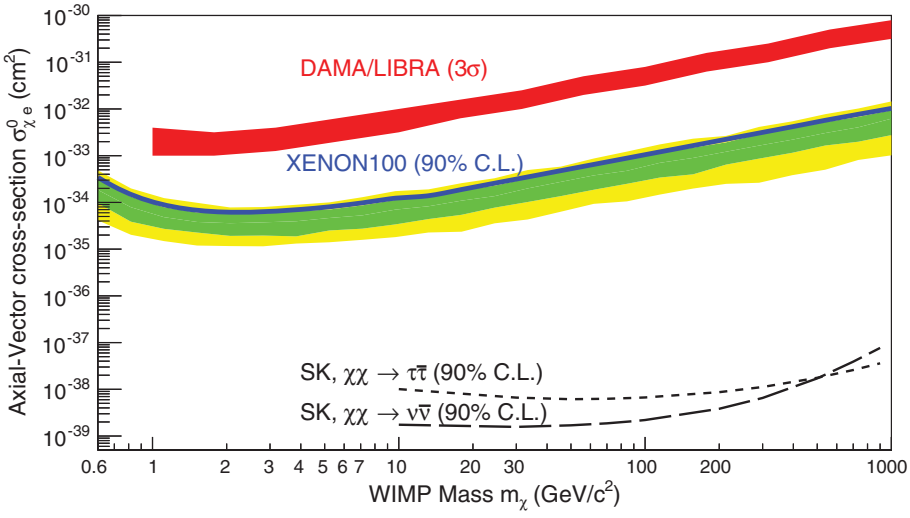

Fig. 4. Parameter space for WIMPs coupling to electrons through axial-vector interactions. The XENON100 upper limit (90% confidence level, C.L.) is indicated by the blue line, along with the green and yellow bands indicating the 1σ and 2σ sensitivity, respectively. For comparison, we also show the DAMA/LIBRA allowed region (red) and the constraint from Super-Kamiokande (SK) using neutrinos from the Sun, by assuming dark matter annihilation into ττ̄ or νν̄, both calculated in (*9*).

of WIMPs coupling to electrons through axial-vector interactions.

It has been suggested that multicomponent models with light dark matter particles of ~MeV/c^2 mass might explain the DAMA/LIBRA modulation (*27*). A specific example of such a model, kinematically mixed mirror dark matter (*28*), was shown to broadly have the right properties to explain the DAMA/LIBRA signal via dark matter–electron scattering. In this model, dark matter halos are composed of a multicomponent plasma of mirror particles, each with the same mass as their standard model partners. The mirror sector is connected to the normal sector by kinetic mixing of photons and mirror photons at the level of ~10^{-9}. Whereas mirror hadrons would not induce nuclear recoils above threshold, mirror electrons ($m_{e'} = 511\,\mathrm{keV}/c^2$) would have a velocity dispersion large enough to induce ~keV electronic recoils.

The differential scattering rate of mirror electrons is proportional to $gNn_{e'}$, where g is the number of loosely bound electrons, assumed to be those with binding energy <1 keV (*28*); N is the number of target atoms; and $n_{e'}$ is the mirror electron density. To compare DAMA/LIBRA directly with XENON100, we apply a constant scaling of $g_{Xe}/g_{NaI} \cdot N_{xe}/N_{NaI} = 0.89$ to the DAMA/LIBRA spectrum and use the same procedure as in the case of axial-vector coupling: We again consider only the DAMA/LIBRA modulation signal, use the 70 summer live days, model scintillation in liquid xenon as described previously, and simply compare integral counts up to the point where the DAMA/LIBRA signal falls below the expected average XENON100 background data rate (at 13 PE), without background subtraction. This excludes the DAMA/LIBRA signal as kinematically mixed mirror dark matter at 3.6σ confidence level.

The third model we consider is luminous dark matter (*29*), featuring a dark matter particle with a ~keV mass splitting between states connected by a magnetic dipole moment operator. The dark matter particle upscatters in the Earth and later de-excites, possibly within a detector, with the emission of a real photon. The experimental signature of this model is a mono-energetic line from the de-excitation photon. A mass splitting δ = 3.3 keV provides a good fit to the DAMA/LIBRA signal (*29*), which would be explained as scattering of a real photon from the de-excitation of a ~GeV/c^2 dark matter particle that is heavy enough to undergo upscattering, but light enough to evade detection in other direct searches.

This signature is independent of the target material; only the sensitive volume affects the induced event rate. As rates are typically given per unit detector mass, scaling to volume is inversely proportional to target density. We thus apply a constant scaling factor to the differential rate in DAMA/LIBRA, which is the ratio of the target densities $\rho_{NaI}/\rho_{Xe} = 1.29$, in order to compare it to XENON100. Proceeding as in the previous two cases, we exclude the DAMA/LIBRA signal as luminous dark matter at 4.6σ confidence level. Together with the other two exclusions presented above, this robustly rules out leptophilic dark matter interactions as a cause for the DAMA/LIBRA signal.

REFERENCES AND NOTES

1. L. Bergström, *Annalen Phys.* **524**, 479–496 (2012).
2. A. K. Drukier, K. Freese, D. N. Spergel, *Phys. Rev. D Part. Fields* **33**, 3495–3508 (1986).
3. K. Freese, M. Lisanti, C. Savage, *Rev. Mod. Phys.* **85**, 1561 (2013).
4. R. Bernabei *et al.*, *Eur. Phys. J. C* **73**, 2648 (2013).
5. C. Savage, G. Gelmini, P. Gondolo, K. Freese, *J. Cosmol. Astropart. Phys.* **0904**, 010 (2009).
6. Y. Bai, P. J. Fox, Resonant dark matter. *J. High Energy Phys.* **0911**, 052 (2009). .
7. S. Chang, N. Weiner, I. Yavin, *Phys. Rev. D Part. Fields Gravit. Cosmol.* **82**, 125011 (2010).
8. S. Chang, R. F. Lang, N. Weiner, *Phys. Rev. Lett.* **106**, 011301 (2011).
9. J. Kopp, V. Niro, T. Schwetz, J. Zupan, *Phys. Rev. D Part. Fields Gravit. Cosmol.* **80**, 083502 (2009).
10. N. F. Bell, Y. Cai, R. K. Leane, A. D. Medina, *Phys. Rev. D Part. Fields Gravit. Cosmol.* **90**, 035027 (2014).
11. E. Aprile *et al.*, *Phys. Rev. Lett.* **109**, 181301 (2012).
12. E. Aprile *et al.*, *Phys. Rev. Lett.* **111**, 021301 (2013).
13. E. Aprile *et al.*, *Phys. Rev. D Part. Fields Gravit. Cosmol.* **90**, 062009 (2014).
14. E. Aprile *et al.*, *Astropart. Phys.* **35**, 573–590 (2012).
15. E. Aprile *et al.*, *Astropart. Phys.* **54**, 11 (2014).
16. E. Aprile *et al.*, *Phys. Rev. D Part. Fields Gravit. Cosmol.* **83**, 082001 (2011).
17. R. Bernabei *et al.*, *Eur. Phys. J. C* **56**, 333–355 (2008).
18. V. Kudryavtsev, M. Robinson, N. Spooner, *Astropart. Phys.* **33**, 91–96 (2010).
19. J. Herrero-Garcia, T. Schwetz, J. Zupan, *J. Cosmol. Astropart. Phys.* **1203**, 005 (2012).
20. R. Bernabei *et al.*, *Phys. Rev. D Part. Fields Gravit. Cosmol.* **77**, 023506 (2008).
21. M. Szydagis *et al. J. Instrum.* **6**, P10002 (2011).
22. A. Manalaysay *et al.*, *Rev. Sci. Instrum.* **81**, 073303 (2010).
23. E. Aprile *et al.*, *Phys. Rev. D Part. Fields Gravit. Cosmol.* **86**, 112004 (2012).
24. L. Baudis *et al.*, *Phys. Rev. D Part. Fields Gravit. Cosmol.* **87**, 115015 (2013).
25. M. Szydagis, A. Fyhrie, D. Thorngren, M. Tripathi, *Instrum.* **8**, C10003 (2013).
26. E. Aprile *et al.*, *Phys. Rev. D Part. Fields Gravit. Cosmol.* **84**, 052003 (2011).
27. R. Foot, H. Lew, R. Volkas, *Phys. Lett. B* **272**, 67–70 (1991).
28. R. Foot, *Int. J. Mod. Phys. A* **29**, 1430013 (2014).
29. B. Feldstein, P. W. Graham, S. Rajendran, *Phys. Rev. D Part. Fields Gravit. Cosmol.* **82**, 075019 (2010).

ACKNOWLEDGMENTS

We thank J. Kopp for providing the calculated wave functions and for useful discussions. We gratefully acknowledge support from the National Science Fundation, Department of Energy, Swiss National Science Foundation, Volkswagen Foundation, Bundesministerium fur Bildung und Forschung, Max Planck Gesellschaft, Research Center Elementary Forces and Mathematical Foundations, Foundation for Fundamental Research on Matter, Weizmann Institute of Science, Initial Training Network Invisibles, Fundacao para a Ciencia e a Tecnologia, Region des Pays de la Loire, Science and Technology Commission of Shanghai Municipality, National Natural Science Foundation of China, and Istituto Nazionale di Fisica Nucleare. We are grateful to Laboratori Nazionali del Gran Sasso for hosting and supporting the XENON project. XENON data are archived at the Laboratori Nazionali del Gran Sasso.

SUPPLEMENTARY MATERIALS

www.sciencemag.org/content/349/6250/851/suppl/DC1
The XENON Collaboration Author List
Data Files A1 and A2

28 March 2015; accepted 25 June 2015
10.1126/science.aab2069

ECOLOGICAL THEORY

A general consumer-resource population model

Kevin D. Lafferty,[1]* Giulio DeLeo,[3] Cheryl J. Briggs,[2] Andrew P. Dobson,[4,5] Thilo Gross,[6] Armand M. Kuris[2]

Food-web dynamics arise from predator-prey, parasite-host, and herbivore-plant interactions. Models for such interactions include up to three consumer activity states (questing, attacking, consuming) and up to four resource response states (susceptible, exposed, ingested, resistant). Articulating these states into a general model allows for dissecting, comparing, and deriving consumer-resource models. We specify this general model for 11 generic consumer strategies that group mathematically into predators, parasites, and micropredators and then derive conditions for consumer success, including a universal saturating functional response. We further show how to use this framework to create simple models with a common mathematical lineage and transparent assumptions. Underlying assumptions, missing elements, and composite parameters are revealed when classic consumer-resource models are derived from the general model.

Malthus (*1*) first postulated that resource availability constrains consumer population growth in 1798. Since then, there have been about 1000 host-parasitoid, 3000 parasite-host, and 5000 predator-prey modeling studies, all describing interactions between consumers and their resources [summarized in (*2*, *3*)]. Here, we show how the seven state variables and associated transitions used in classic models can comprise a general consumer-resource model that underlies the structure of all ecological food webs (*4*). The general model describes population rates of change for searching, or questing, (Q); handling, or attacking, (A); and feeding or consuming (C) activity states of consumers and the

Exclusion of leptophilic dark matter models using XENON100 electronic recoil data

The XENON Collaboration (August 20, 2015)
Science **349** (6250), 851-854. [doi: 10.1126/science.aab2069]

Editor's Summary

Limiting unknows in the dark side

Our knowledge of the inventory of stuff that makes up our universe amounts to a humbling 5%. The rest consists of either dark energy (~70%) or dark matter (~25%). Using atom interferometry, Hamilton *et al.* describe the results of experiments that controlled for dark energy screening mechanisms in individual atoms, not bulk matter. Aprile *et al.* report on an analysis of data taken with the XENON100 detectors aiming to identify dark matter particles directly by monitoring their rare interaction with ordinary matter. In this setup, a large underground tank of liquid xenon forms a target for weakly interacting m assive particles. These combined results set limits on several types of proposed dark matter and dark energy candidates (see the Perspective by Schmiedmayer and Abele).

Science, this issue p. 849, p. 851; see also p. 786